ISSN 1392-1207. MECHANIKA. Vol. 32, No. 3, 2026: 195–207

# Design Improvement of Unloading Groove Structure for Fluid Dynamic Performance of External Gear Pumps

**Jiachen TANG*, Mengyuan LAN**, Liang ZHAO**, Shibiao ZHANG**, Jianhua YANG**, Zhen SHAN*****

*Xuzhou Heavy Machinery Co., Ltd., Xuzhou 221004, China
**School of Mechanical and Electrical Engineering, China University of Mining and Technology, Xuzhou 221116, China, E-mails: mengyuanlan@cumt.edu.cn; 2177@cumt.edu.cn (Corresponding Author: Liang Zhao)
***School of Computer Science and Technology, China University of Mining and Technology, Xuzhou 221116, China

https://doi.org/10.5755/j02.mech.42331

## 1.Introduction

Hydraulic systems are widely utilized in mechanical engineering due to their high power density, flexible configuration, and precise control capabilities. Among various hydraulic components, the external gear pump is a positive displacement device that transfers fluid via meshing gears. These pumps are favored for their simple and compact structure, low manufacturing cost, reliable performance, and relatively high volumetric efficiency [1]. Their stable operation under diverse working conditions has led to widespread applications in automotive, aerospace, medical, and industrial fields [2-4].

However, external gear pumps often exhibit significant flow and pressure pulsations during operation, especially under high-pressure and high-speed conditions [5, 6]. Such pulsations can lead to increased system vibration and noise, affecting both stability and efficiency [7]. Two key structural features that influence these phenomena are tooth backlash and the unloading groove [8-10]. Tooth backlash affects fluid leakage and flow stability, while the unloading groove plays a critical role in mitigating trapped oil pressure and cavitation.

This study employs PumpLinx software to perform fluid dynamic simulations of external gear pumps with various unloading groove configurations and meshing conditions. A Curved unloading groove design is proposed and evaluated both in the presence and absence of tooth backlash. The simulation results provide insights into optimizing pump geometry to reduce flow pulsation and enhance volumetric efficiency.

There have been some extensive researches on this topic, especially on design of unloading grooves. Zhang et al. investigated the effect of unloading groove spacing and mainly considered on the performance of the transient multi flow field of an external gear pump [11]. They found that reducing the unloading groove spacing can appropriately reduce flow pulsation and improve volumetric efficiency. Zhan et al. studied the noise characteristics of a high-speed gear pump and added an oil replenishment groove to reduce the flow pulsation [12]. Liu et al. developed a fuel gear pump based on aviation engines, and studied the internal flow field by establishing a stagnation calculation model. They proposed a novel design method for the discharge groove of the engine fuel gear pump in the light of square discharge groove [13]. Sedri et al. carried out numerical, analytical, and experimental investigations on a simple external gear pump, introducing a new group of unloading slots on the gear teeth to improve the performance of the pump [14]. They also investigated the effects of gear radius and tooth tip length on pump performance.

Some scholars have also conducted researches on the influence of tooth backlash on flow pulsation. Gamez Montero et al. added a minimum gap module and an overflow channel effective port area module to GeroLAB's structured method to increase the efficiency of the cycloidal pump [15]. Szwemin et al. introduced the simulation results of axial and radial clearance leakage of external meshing pumps for different geometric shapes, sizes, and operating parameters [16]. Under the preconditions of various of radial and end clearances, Zhan et al. studied the influences of the oil leakage flow rate as well as the pump shaft power, and determined the optimal solutions for the end face together with the radial clearance of the high-speed gear pump [17]. Gamez et al. considered the effect of different tooth clearances on the flow pulsation of cycloidal pumps and obtained beneficial laws [18].

The above works mainly focus on improving the performance of gear pumps unilaterally by optimizing the design of the unloading groove or only conducting experimental analysis on the performance of pumps with different tooth backlashs. This work aims to optimize and improve the performance of an external gear pump by a novel type of unloading groove in the presence or absence of tooth backlash. Based on conducting fluid simulation analysis and comparison using PumpLinx software, we verify the optimization results through comparative analysis of multiple parameters such as the trapped oil pressure, the flow pulsation, and the flow non-uniformity coefficient. This study provides industry professionals with different choices of external gear pumps in the light of various factors such as actual working conditions and needs, and also serves as a reference for engineers in optimizing the dynamics performance of an external gear pump.

## 2. Analysis of Oil Trapping Mechanism in External Gear Pumps

### 2.1. Trapped oil mechanism and function of the unloading groove in external gear pumps

During operation, external gear pumps rely on the meshing of gear pairs to drive periodic changes in the working chamber volume, thereby enabling fluid suction and discharge [19]. Due to the overlapping meshing process—where one pair of teeth has not yet completely disengaged

while another pair is already entering engagement—a temporarily sealed chamber is formed between adjacent teeth. This chamber is intermittently isolated from both the suction and discharge ports and periodically forms and disappears as the gears rotate. Because the fluid within this sealed chamber cannot exchange with the external flow field in a short time, pressure fluctuations occur as the chamber volume changes. This phenomenon is commonly referred to as the trapped oil effect [20, 21].

The trapped oil effect is an inherent fluid dynamic phenomenon in external gear pumps, arising from the compression or expansion of fluid within a closed volume. When side clearance exists, two initially independent trapped oil regions may become connected through the clearance, forming a single combined trapped oil region.

By taking the gear rotation angle as the independent variable, the variation of the trapped volume can be approximately described as

$$V(\theta) = V_0 - k_v \theta, \tag{1}$$

where $V$ denotes the trapped volume of the working chamber, $V_0$ is the initial trapped volume, $k_v$ is the volume variation coefficient, and $\theta$ represents the gear rotation angle. The rate of change of the trapped volume can be expressed as

$$\frac{dV}{dt} = \frac{dV}{d\theta}\omega, \tag{2}$$

where $\omega$ denotes the angular velocity.

When the volume of the sealed chamber decreases, the fluid is compressed, leading to a rapid increase in pressure. Conversely, when the volume expands, the fluid undergoes expansion, resulting in a pressure drop and even local negative pressure. Considering the finite compressibility of the fluid, the pressure variation can be described using the bulk modulus relationship

$$\beta = -V\frac{dP}{dV}, \tag{3}$$

where $\beta$ is the bulk modulus.

Due to fluid compressibility, rapid volume variation within a short time leads to significant pressure fluctuations, which directly affect the operational stability of the gear pump. The pressure evolution in the trapped oil region can thus be approximated as a control-volume compression process

$$\frac{dP}{dt} = -\beta\frac{1}{V}\frac{dV}{dt}. \tag{4}$$

The peak pressure of the trapped oil region can be estimated based on the compression relationship

$$P_{max} = P_0 + \beta ln\left(\frac{V_0}{V}\right), \tag{5}$$

where $P_0$ is the initial pressure.

This relationship indicates that pressure variation is closely related to the rate of volume change. When the gear rotation causes a rapid decrease in the trapped volume ($dV/dt < 0$), the pressure rises sharply, forming a local high-pressure region. If not released in time, this may induce hydraulic shock, affecting gear meshing conditions and structural loading.

To alleviate the above issues, unloading grooves are typically machined on the front and rear covers, bearing seats, or floating side plates of gear pumps. The introduction of the unloading groove essentially provides a transitional channel for the trapped volume, enabling gradual pressure release or compensation before the gear chamber connects to the high- or low-pressure regions. As a result, the pressure gradient is smoothed, and the abrupt pressure variation in the trapped oil region is effectively mitigated, transforming the pressure evolution from an “abrupt-type” to a “gradual-type” behavior.

This design allows high-pressure fluid to be discharged into the groove during the compression phase, while enabling fluid re-entry during the expansion phase. This pressure balancing mechanism plays two key roles in the pressure evolution process

1. Volume compensation effect

When the trapped volume decreases, the unloading groove allows part of the fluid to flow prematurely toward the high-pressure chamber, reducing the effective compression ratio. When the volume increases, low-pressure fluid is supplemented in advance, preventing the formation of negative pressure. In this way, the unloading groove modifies the connectivity timing of the trapped volume, resulting in a smoother pressure profile.

2. Throttling and damping effect

The unloading groove has a limited cross-sectional area and essentially behaves as a transient throttling orifice. The flow rate can be approximated as

$$Q_s = C_d A_{eff}\sqrt{\frac{2\Delta P}{\rho}}, \tag{6}$$

where $Q_s$ denotes the flow rate through the unloading groove, $C_d$ is the discharge coefficient, $A_{eff}$ is the effective flow area of the groove opening, $\Delta P$ represents the pressure difference between the trapped volume and the high/low-pressure chambers, and $\rho$ is the fluid density.

A larger throttling area leads to faster pressure relief; however, an excessively large area may cause premature direct connection between the high- and low-pressure chambers, resulting in increased internal leakage. Therefore, the design of the unloading groove essentially involves achieving a balance among throttling area, connection timing, and pressure smoothing performance.

The geometric parameters of the unloading groove, including groove width, depth, and opening/closing angles, directly determine its throttling capacity and discharge timing. Consequently, they significantly influence the transient pressure peaks in the trapped oil region, outlet flow pulsation intensity, radial hydraulic force imbalance, as well as internal leakage and volumetric efficiency. The effective flow area can be expressed as

$$A_{eff} = b_s l_s, \tag{7}$$

where $b_s$ and $l_s$ are the groove width and length, respectively.

From the perspective of pressure evolution, the presence of the unloading groove is equivalent to introducing an additional pressure relief channel between the trapped oil region and the external oil chambers. When the discharge effect of the unloading groove is considered, the pressure variation equation in the trapped oil region can be expressed as

$$\frac{dp}{dt} = -\beta \frac{1}{V}\left(\frac{dV}{dt} - Q_s\right). \tag{8}$$

This expression indicates that when the unloading groove provides sufficient discharge capacity, the pressure fluctuations induced by the variation of the trapped volume can be effectively alleviated, thereby reducing the peak pressure in the trapped oil region.

In summary, the trapped oil phenomenon originates from the periodic variation of the sealed volume during gear meshing. The unloading groove structure regulates the pressure evolution process by modifying the connectivity conditions between the trapped chamber and the external oil passages. A properly designed unloading groove not only reduces the trapped oil pressure peak but also improves the internal flow characteristics of the pump, thereby providing an important theoretical basis for the structural design and improvement of external gear pumps.

## 2.2. Design theory of unloading groove opening angle and length

Based on the trapped oil mechanism, the opening angle and length of the unloading groove are critical design parameters determined by the gear meshing geometry. The key step in the groove design is to determine the minimum unloading groove spacing, which is governed by the length of the trapped oil region generated during gear meshing, as shown in Fig. 1. Since the trapped oil region varies with the meshing position, the groove spacing must be sufficiently large to completely cover the trapped oil region while preventing premature connection between the high- and low-pressure chambers. Therefore, the calculation of the minimum unloading groove spacing serves as the theoretical foundation for determining the geometric parameters of the Curved unloading groove and establishes a direct link between the theoretical analysis and the actual groove design procedure adopted in this study.

The contact between gear teeth occurs along the line of action. According to involute gear theory, the contact line length is given by

$$L = \sqrt{r_a^2 - r_b^2} + \sqrt{r_a^2 - r_b^2} - a\sin\alpha, \tag{9}$$

where $r_a$, $r_b$, $a$, and $\alpha$ denote addendum radius, base circle radius, center distance, and pressure angle, respectively.

$$\varepsilon = \frac{L}{P_b}, \tag{10}$$

where

$$P_b = \pi m \cos\alpha \tag{11}$$

is base pitch, and $m$ is a module.

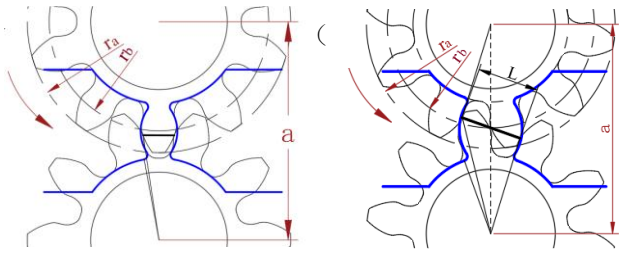


a b

Fig. 1 Design and optimization of unloading groove: a – zero-backlash gear pair, b – gear pair with backlash

When $\varepsilon > 1$, two pairs of teeth are simultaneously engaged, forming a trapped volume. This region typically forms near the middle of the contact line and enters compression as rotation proceeds.

Let the pitch circle radius of the gear be $r$. Based on the gear meshing geometry, the pitch angle corresponding to the onset of trapped volume compression can be approximated as

$$\theta_c = \frac{P_b}{2r}. \tag{12}$$

To ensure timely pressure relief of the trapped oil, the unloading groove should establish communication with the high-pressure chamber before the compression phase begins. Therefore, the opening angle of the unloading groove should satisfy

$$\theta_s \approx \theta_c - \Delta\theta, \tag{13}$$

where $\Delta\theta$ is a safety advance angle, typically chosen as a small value to ensure stable pressure release.

The angular range during which the trapped volume exists can be expressed as

$$\Delta\theta_c = (\varepsilon - 1)\frac{P_b}{r}. \tag{14}$$

As the contact point moves along the line of action, the corresponding arc displacement on the pitch circle is given by

$$l_c = r\Delta\theta_c. \tag{15}$$

Since the unloading groove must cover the main angular range of the trapped volume, its length is generally designed as

$$l_s \approx l_c. \tag{16}$$

In practical engineering design, to prevent excessive unloading groove length that may lead to premature leakage of high-pressure fluid, the theoretically derived groove length is usually modified by introducing a correction factor $k_l$, which is generally less than 1. The introduction of this correction factor enables a balance between trapped oil pressure relief and volumetric efficiency preservation. Therefore, the minimum unloading groove spacing without gear backlash can be obtained as:

$$l_s = k_l (2P_b - L)\cos\alpha, \tag{17}$$

the minimum spacing of the unloading grooves in the presence of gear backlash is given by:

$$l_b = k_l P_b \cos\alpha \ . \tag{18}$$

Based on the above analysis, the main geometric parameters of the unloading groove include the opening angle, groove length, width, depth, and profile. The selection of these parameters requires a trade-off between trapped oil pressure relief and volumetric efficiency. If the groove opens too early or has an excessively large area, high-pressure fluid may leak prematurely into the low-pressure region, increasing internal leakage and reducing volumetric efficiency. Conversely, if it opens too late, the trapped oil pressure cannot be effectively relieved. Therefore, in gear pump design, the starting position, size, and relative position of the unloading groove with respect to the gear meshing region should be properly determined to ensure timely pressure release during compression while minimizing unnecessary leakage. Accordingly, the parameter range should be determined through a combination of theoretical analysis and numerical simulation.

### 2.3. Structural analysis and optimization of unloading grooves

The hydraulic system of the new energy crane studied in this work employs an external spur gear pump. The pump mainly consists of a pair of driving gears, a pump housing, bearings, and floating side plates. The floating side plates not only provide axial sealing and clearance compensation, but also serve as the mounting location for the unloading grooves. The unloading grooves are machined on the transitional region of the floating side plates on both sides of the gears. Their primary function is to regulate the pressure evolution of the trapped volume during gear meshing, thereby alleviating the trapped oil effect and reducing internal pressure shocks and flow-induced excitation.

The studied external gear pump exists in two manufacturing precision levels. For high-precision gears, the side clearance is extremely small and can be approximately regarded as a zero-clearance configuration. For lower-precision manufacturing, a certain side clearance exists due to machining and assembly errors. However, both configurations adopt the same unloading groove design. Since the side clearance directly affects the connectivity and pressure relief path of the trapped volume, it is necessary to evaluate the applicability of the original groove design under different assembly conditions. Accordingly, two 3D models—namely “zero side clearance” and “with side clearance”—are established to analyze and optimize the unloading groove parameters under each condition.

Under the zero side clearance condition, the non-working tooth surfaces are tightly engaged, and the trapped volume is divided into two relatively independent regions during meshing transition. As shown in Fig. 2, a, since the original unloading groove only connects to one region, the other remains fully sealed within a certain angular range. As the gears rotate and the volume decreases, fluid in the sealed chamber is compressed, leading to a rapid pressure rise. Even if pressure is released in the connected region, the isolated region still generates high transient pressure peaks, resulting in uneven load distribution and increased radial hydraulic force fluctuation. Therefore, under zero-clearance

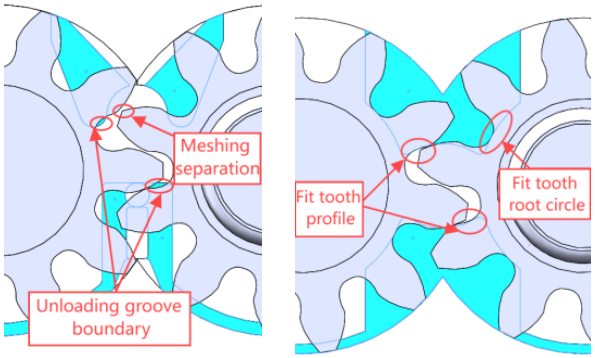


Fig. 2 Original unloading groove structure analysis: a – zero-backlash gear pair, b – gear pair with backlash

conditions, the original groove design exhibits insufficient pressure relief capability.

Under the side clearance condition, a micro-gap channel is formed between the non-working tooth surface and the side plate, providing an additional leakage path for the trapped volume. However, the original groove opening and closing angles do not account for this effect. During certain meshing stages, the unloading groove may simultaneously connect the inlet and outlet chambers, forming a cross-chamber flow path, as shown in Fig. 2, b. In this case, high-pressure fluid may leak back to the low-pressure chamber through both the groove and the side clearance, resulting in unnecessary internal leakage. This not only reduces volumetric efficiency but also disturbs the internal flow field and increases flow fluctuation.

Based on the above analysis, the unloading groove design is optimized from three aspects: dimensional matching, structural configuration, and connectivity timing. The objective is to ensure effective pressure relief of the trapped oil region under both side-clearance and zero-clearance conditions while avoiding abnormal communication between the inlet and outlet chambers.

For dimensional design, the opening and closing positions, axial layout, and minimum spacing of the unloading grooves are determined according to the meshing characteristics of the gear pair and the dynamic evolution of the trapped oil region. The design principle is that when the trapped oil region disengages from the discharge-side unloading groove, it should immediately establish communication with the suction-side unloading groove. In this way, pressure release can proceed continuously and controllably, preventing excessive compression of the trapped volume and suppressing the generation of high pressure peaks.

For the optimized external gear pump investigated in this study, the gear parameters are: number of teeth $z = 10$, module $m = 4.5$ mm, and pressure angle $\alpha = 20°$. Substituting these parameters into Eqs. (2)-(9) – (2)-1(8), the addendum circle radius, base circle radius, meshing line length, base pitch, and contact ratio are calculated as $r_a = 27$ mm, $r_b = 21.14$ mm, $L = 18.19$ mm, $P_b = 13.28$ mm, and $\varepsilon = 1.369$, respectively. Based on the theoretical trapped-oil analysis, the minimum unloading groove spacing is determined to be 7.94 mm under zero-clearance conditions and 12.6 mm when side clearance is considered. These values provide the theoretical basis for the subsequent groove dimension design and ensure proper matching between the

unloading groove and the trapped oil region during the meshing process.

As shown in Fig. 3, a, in the original design, identical asymmetric unloading grooves with a depth of 1 mm and a minimum spacing of 9.1 mm are adopted regardless of whether side clearance exists. Under side-clearance conditions, the groove spacing is smaller than the theoretically required minimum spacing of 12.6 mm, causing premature communication between the inlet and outlet chambers through the unloading grooves, which increases internal leakage and reduces volumetric efficiency. Conversely, under zero-clearance conditions, the groove spacing exceeds the theoretically required value of 7.94 mm, delaying the establishment of communication between the trapped oil region and the unloading groove. As a result, the trapped volume continues to be compressed, leading to excessive trapped-oil pressure and pressure fluctuations.

To address these issues, optimized unloading grooves are designed separately for the side-clearance and zero-clearance conditions while maintaining the same overall geometric concept. The minimum groove spacing is adjusted to 12.6 mm and 7.94 mm, respectively, according to the theoretical calculations. In addition, a symmetric groove arrangement is adopted on both sides of the gear, and a circular transition with a diameter of 33.75 mm is introduced to match the gear root circle profile. This design increases the effective overlap area between the trapped oil region and the unloading groove, shortens the pressure-relief path, improves the timing of pressure release, and prevents abnormal cross-chamber flow, as shown in Fig. 3, b and c.

Furthermore, the optimized curved unloading groove employs a trapezoidal cross-section instead of the conventional rectangular configuration. Owing to its gradually expanding flow area, the trapezoidal structure reduces sudden velocity changes and local flow separation, thereby weakening vortex formation and lowering the risk of cavitation. The smoother pressure transition contributes to reduced flow pulsation, lower vibration and noise levels, and improved load distribution between the gear teeth and side plates.

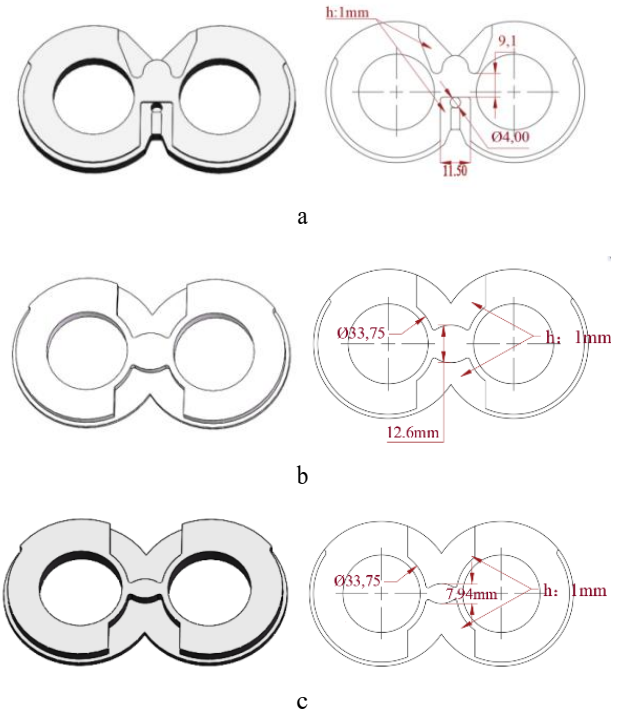


Fig. 3 Unloading groove model before and after structural optimization: a – irregular-shaped unloading groove, b – curved unloading groove with tooth backlash, c – curved unloading groove without tooth backlash

For the zero-backlash condition, the optimized structure adopts a symmetric configuration. An unloading groove with identical geometry is added on the suction side to mirror the one on the discharge side. When one trapped chamber connects with the discharge side groove, the other independent trapped chamber can simultaneously connect with the suction side groove. This prevents the formation of isolated high-pressure chambers and enables synchronous pressure relief of both chambers, resulting in a more balanced pressure distribution, as shown in Fig. 4.

For the side backlash condition, the optimization focuses on controlling the connectivity timing. When the trapped region connects with the suction side groove, it should be disconnected from the discharge side groove in time. By adjusting the minimum spacing between the two grooves to be greater than or equal to the maximum extended length of the dual trapped regions, a direct flow path between inlet and outlet chambers is structurally blocked. This suppresses backflow, improves volumetric efficiency, and reduces the amplitude of flow and pressure pulsations.

Overall, the proposed design ensures effective trapped oil relief under both operating conditions by improving pressure synchronization and regulating flow connectivity, thereby enhancing the hydraulic stability of the gear pump.

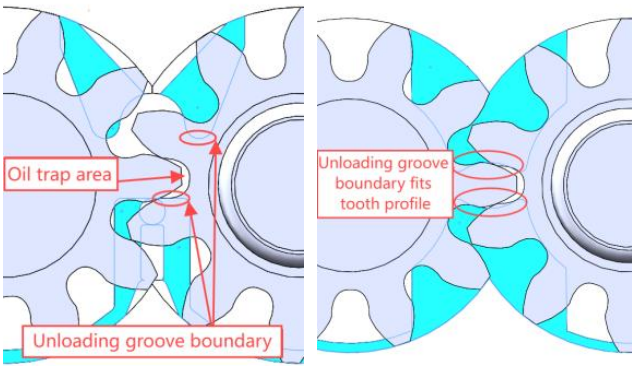


Fig. 4 Curved unloading groove structure analysis: a – zero-backlash gear pair, b – gear pair with backlash

## 3. Fluid Simulation Analysis of an External Gear Pump

Regarding external gear pumps, this study performs computational fluid dynamics (CFD) simulations for both the original unloading groove design and the improved unloading groove design, under conditions where the gear pair meshing exhibits backlash and under idealized meshing (zero clearance). Based on the simulation results, a comparative analysis is conducted on the influence patterns of these two designs on key performance parameters of the pump, specifically the inlet/outlet flow pulsation and trapped oil pressure. The simulation workflow is depicted in Fig. 5.

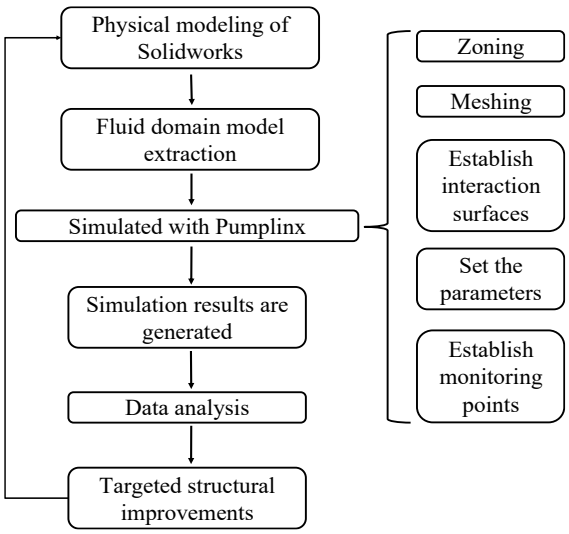


Fig. 5 Flowchart for fluid dynamics simulation of an external gear pump

### 3.1. Physical model establishment of the external gear pump

The concrete steps for establishing a physical model of the external gear pump are as follows.

Gears serve as the core transmission components within an external gear pump, primarily responsible for fluid conveyance. Fluid suction, compression, and discharge are accomplished through the continuous meshing and rotation of a gear pair, typically comprising a driving gear mounted on the input shaft and a driven gear on the output shaft. As the gears rotate, enclosed chambers are formed between the meshing teeth, allowing the fluid to be entrapped, pressurized, and expelled accordingly [22, 23].

By using the software SOLIDWORKS to establish different external meshing gears, the gear pump studied in this article is divided into two types, i.e., gear meshing without backlash and gear meshing with backlash, By increasing the center distance between the two external gears, then the gear set without backlash is converted into a gear set with backlash.

SOLIDWORKS was utilized to construct two representative gear configurations: one without backlash, representing ideal precision conditions, and another with designed backlash to reflect typical manufacturing tolerances. Tooth backlash was implemented by reducing the tooth thickness of the gears, not only simulates assembly clearances but also reflects real-world manufacturing deviations.

Table 1 outlines the core meshing parameters, such as module, tooth count, and center distance, all of which significantly influence the sealing performance and trapped oil behavior of the pump.

Table 1

Gear meshing parameters

| | Without backlash | With backlash |
|---|---|---|
| Modulus | 4.5 | 4.5 |
| Number of teeth | 10 | 10 |
| Tooth thickness, mm | 7.069 | 7.059 |
| Tooth width, mm | 23 | 23 |
| Addendum circle clearance, mm | 0.01 | 0.01 |

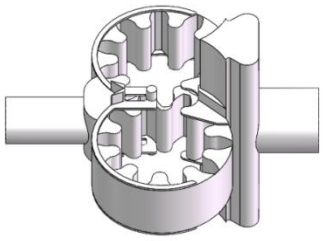

Fig. 6 Gear pump fluid domain model

Based on the working principle of PumpLinx software, fluid simulation requires extracting the fluid domain model of the gear pump. This section takes the gear pump with a tooth backlash shaped unloading groove as an example, and extracts the fluid domain of different types of gear pumps through Boolean operations in SOLIDWORKS software. The fluid domain model of the external gear pump is presented in Fig. 6.

### 3.2. Import and pre-processing of fluid domain model

There are mainly five steps to import and preprocess of the fluid domain model:

1. Regional division.

Convert the fluid domain model extracted in SOLIDWORKS to “stl” format and import it into PumpLinx software. Then, in PumpLinx software, divide the fluid domain model of the external gear pump into three parts: the inlet area, the gear meshing area, and the outlet area.

2. Grid division.

Generally, flexible grid partitioning is performed based on the geometric shape and flow field characteristics of the fluid domain to better adapt to complex geometric shapes, reduce the number of grids and computational complexity, and better handle boundary conditions, thereby improving the accuracy, stability, and efficiency of simulation.

This work uses the General Mesher and Rotor Template Mesher functions that come with PumpLinx to input boundary conditions, mesh size, and other parameters to achieve universal mesh partitioning of the inlet and outlet

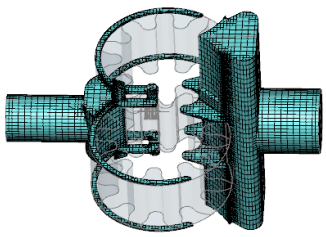

a

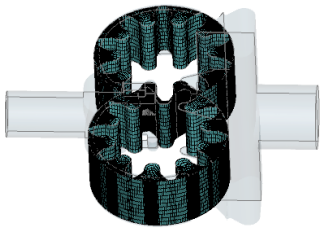

b

Fig. 7 Grid division in different regions: a – grid of inlet and outlet areas, b – grid of gear meshing area

areas and dynamic mesh partitioning of the gear meshing area, as illustrated in Fig. 7

3. Interactive surface creation.

Following the generation of general meshes for the inlet and outlet regions and dynamic meshes for the gear meshing area, it is necessary to define interaction surfaces due to differences in mesh density and type across these zones. These interfaces enable accurate fluid exchange between regions and allow the simulation to capture multiscale flow characteristics effectively [24]. The final comprehensive interaction surface layout is shown in Fig. 8.

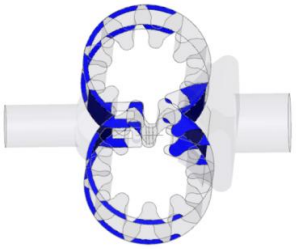

Fig. 8 Interaction surface area

4. Parameter settings.

To ensure that the numerical results accurately reflect the actual operating conditions of the gear pump, the proper definition of boundary conditions is essential. In this study, transient simulations of the gear pump under rated operating conditions were conducted using the PumpLinx platform. The boundary conditions were defined in accordance with experimental measurements and practical engineering conditions.

The gear motion was modeled as rigid-body rotation. The driving gear rotates counterclockwise at a speed of 1200 r/min based on the experimental setup, while the driven gear rotates synchronously through gear meshing constraints. Considering that the experimental rig adopts an open-tank suction system, the inlet boundary was set to atmospheric pressure of 0.1 MPa, and the outlet pressure was set as a high-pressure regulated boundary condition.

The working fluid is a commercial 46# anti-wear hydraulic oil used in this study, with a density of 850 kg/m³, temperature of 35°C, and dynamic viscosity of 0.02993 Pa·s. The effective bulk modulus was set to $1.5 \times 10^9$ Pa. To accurately capture pressure spikes in the trapped oil region, a compressible flow model was enabled. A volumetric air content of 0.5% was considered, and the outlet pressure was adjusted and specified according to the actual operating conditions.

To determine the flow regime, the Reynolds number is evaluated under rated operating conditions. In gear pumps, the characteristic velocity is defined as the circumferential speed of the gear pitch circle, while the characteristic length is taken as the gear module. The Reynolds number is therefore expressed as

$$Re = \frac{\rho m n_{rpm}}{\mu}, \tag{19}$$

where $n_{rpm} = \pi dn/60$, $\rho$ is the fluid density, $\mu$ is the dynamic viscosity, and $m$ is the gear module. Based on the operating condition of 1200 r/min and the physical properties of the hydraulic oil, the calculated Reynolds number exceeds the laminar–turbulent transition range commonly observed in internal gear pump flows. Therefore, a turbulence model is employed in the CFD simulation.

The general specific parameters of the gear pump set in this article are given in Table 2.

The general specific parameters of the medium oil setting are shown in Table 3.

5. Establishment of monitoring points.

Due to the need to detect the pressure pulsation in the trapped oil area, it is necessary to establish dynamic monitoring points in the trapped oil area of the gear pump to obtain the characteristic value and characteristic curve of a specific point in the fluid domain of the gear pump during the simulation process, as shown in Fig. 9. Three trapped area monitoring points are established in the figure.

Table 2

Mechanical parameters

| Attribute | Parameters |
|---|---|
| Number of rotations | 4 |
| Number of gear teeth | 10 |
| Direction of rotation | Anticlockwise |
| Revolution speed, rpm | 1200 |

Table 3

Oil parameters

| Attribute | Parameters |
|---|---|
| Oil temperature, °C | 35 |
| Dynamic viscosity, Pa·s | 0.02993 |
| Density, kg/m³ | 850 |
| Inlet pressure value, MPa | 0.1 |
| Volumetric air content | 0.5% |

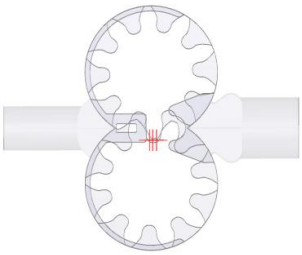

Fig. 9 Establishment of monitoring points

### 3.3. Mesh independence validation

Mesh quality has a direct impact on the accuracy and stability of numerical simulations. For internal flow problems in gear pumps involving dynamic meshing and cyclic variation of the trapped volume, excessively coarse meshes may fail to capture transient pressure peaks in the trapped oil region and local flow gradients. Conversely, overly refined meshes significantly increase computational time per time step and the total number of solver iterations, resulting in excessive computational cost with limited improvement in accuracy. Therefore, selecting an appropriate mesh resolution while ensuring convergence of key physical quantities is a necessary step in numerical modeling.

To verify the suitability of the mesh used in this study, a systematic mesh independence analysis was performed. Mesh independence refers to the condition in which further mesh refinement leads to negligible changes in the computed results, satisfying

$$\frac{\phi_{i+1}-\phi_i}{\phi_{i+1}} < \sigma_\phi , \tag{20}$$

where $\phi_i$ denotes the characteristic physical quantity under the $i$-th mesh level, and $\sigma_\phi$ represents the allowable error threshold. In this study, a value of 1% is adopted as the convergence criterion.

Taking the external gear pump model without side clearance as an example, four mesh configurations with different densities were generated by adjusting the maximum and minimum element sizes, denoted as Mesh I, Mesh II, Mesh III, and Mesh IV. As the mesh level increases, the total number of elements increases accordingly. In particular, finer discretization is applied in the meshing region, the inlet and outlet zones, and the unloading groove region to improve the resolution of pressure gradient variations.

Table 4

Mesh density parameter settings

| | | Mesh I | Mesh II | Mesh III | Mesh IV |
|---|---|---|---|---|---|
| General Mesher | Minimum cell size | 0.002 | 0.0012 | 0.0004 | 0.0002 |
| | Maximum cell size | 0.1 | 0.06 | 0.02 | 0.01 |
| | Curved cell size | 0.05 | 0.03 | 0.01 | 0.005 |
| Rotor Template Mesher | Cells in Rotationl Direction | 180 | 360 | 360 | 360 |
| | Cells in Radial Direction | 4 | 6 | 8 | 10 |
| | Cells in Axial Direction | 8 | 10 | 12 | 14 |

Under identical boundary conditions and solver settings, transient simulations were performed for the four mesh cases. By segmenting the pressure history over a representative cycle, the instantaneous maximum pressure during each trapped-oil formation and compression stage, $P_{max,i}$, was extracted. The cycle-averaged peak pressure of the trapped oil region, $\bar{P}_{max}$, is defined as

$$\bar{P}_{max} = \frac{1}{N_i}\sum_{i=1}^{N} P_{max,i} , \tag{21}$$

where $N_i$ denotes the number of trapped-oil formation events within the statistical cycle.

Comparisons are then performed among the extracted instantaneous peak pressure values, the cycle-averaged peak pressure, and the time-averaged flow rate obtained from the simulations.

As shown in Figs. 10-12, by comparing the peak pressure curves in the trapped oil region, as well as the variations in the mean trapped-oil pressure and the time-averaged outlet flow rate under different mesh densities, the mesh convergence can be evaluated. The peak pressure curves obtained using Mesh III and Mesh IV show good agreement. When refining the mesh from Mesh III to Mesh IV, the variation rate of the mean trapped-oil pressure is 0.939%, and that of the mean outlet flow rate is 0.346%. Both remain within the acceptable error range, indicating that the numerical results have reached a stable state. Further mesh refinement has a negligible impact on the results but leads to a significant increase in computational cost.

Considering both accuracy and efficiency, Mesh III is selected as the standard mesh for subsequent simulations. This mesh provides sufficient accuracy in predicting trapped-oil pressure peaks and flow characteristics while maintaining a reasonable computational cost, thus ensuring a reliable numerical foundation for further fluid dynamic analysis of the gear pump.

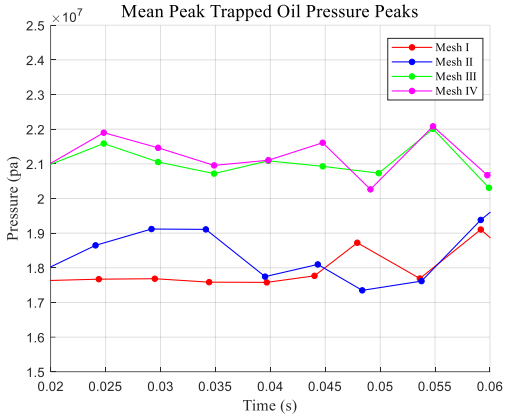


Fig. 10 Trapped oil Pressure peaks under different mesh types

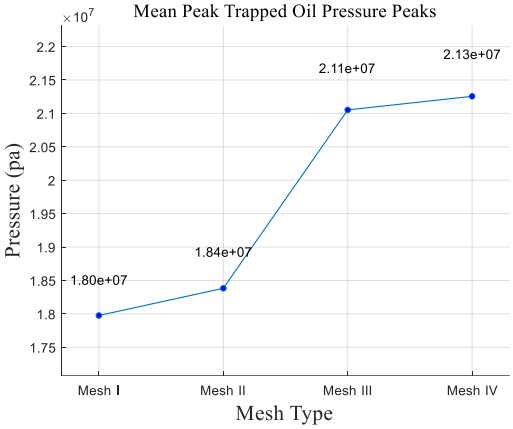


Fig. 11 Mean peak trapped oil pressure peaks under different mesh types

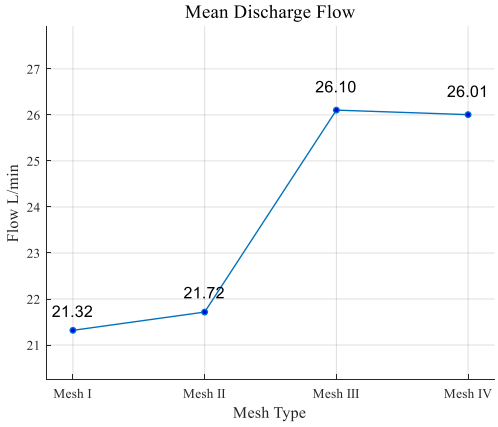


Fig. 12 Mean discharge flow under different mesh types

## 4. Analysis of Simulation Results

For gear pumps with two different unloading groove geometries, modeled both with and without tooth backlash, the corresponding fluid domain models are imported into PumpLinx for simulation. Upon completion of the simulation, critical output data—including flow pulsation, pressure contour maps, and pressure curves at the inlet and outlet—are extracted under defined working conditions. These results are subsequently analyzed and compared to assess the impact of groove geometry and backlash presence on pump performance.

### 4.1. Data analysis of pressure

In Fig. 13, the pressure cloud maps are utilized to evaluate the internal pressure distribution of various gear pump configurations. Specifically, this study selects cloud maps covering the entire meshing cycle—from the initiation of gear contact and the formation of the trapped oil zone to the disengagement phase where the trapped oil zone is released. By analyzing these visualized pressure fields in conjunction with pressure curves recorded at monitoring points within the trapped oil region, a comprehensive comparison of internal pressure behavior under different structural conditions is performed.

As shown in Fig. 14, when the Irregular-shaped unloading groove is applied in the absence of tooth backlash, the trapped oil region is divided into two isolated enclosed chambers. Due to the lack of pressure relief in one of the

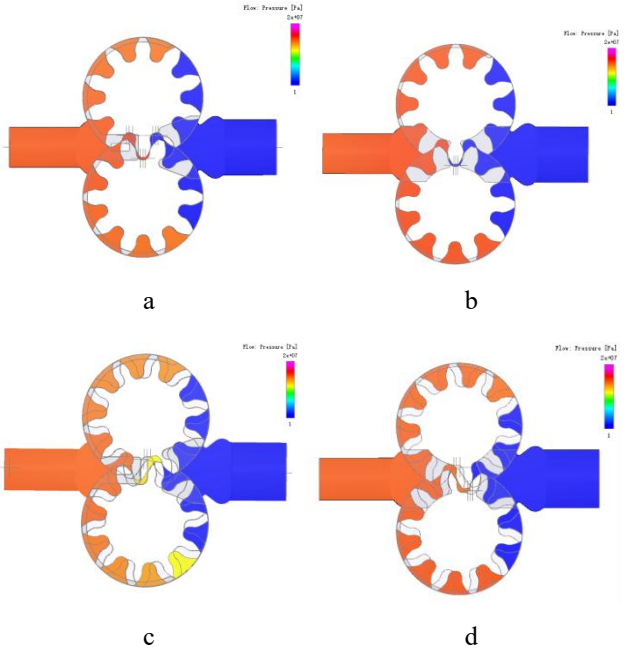


Fig. 13 Contours of fluid pressure for different gear pumps: a – fluid pressure contour diagram of irregular-shaped unloading groove without backlash, b – fluid pressure contour of curved unloading groove without backlash, c – contour of fluid pressure in profiled unloading groove with backlash, d – fluid pressure contour of the curved unloading groove with backlash

chambers during operation, severe pressure buildup occurs, indicating the presence of an intensified oil entrapment effect. This situation arises because when one chamber connects to the outlet, the other remains sealed, preventing timely pressure dissipation. In contrast, the Curved unloading groove – featuring a symmetrical configuration and optimized groove spacing – ensures that both trapped oil regions can sequentially communicate with the suction and discharge ports. This configuration significantly improves the pressure relief process, lowers peak pressure, and reduces the severity of oil entrapment.

In the presence of tooth backlash, the Irregular-shaped unloading groove introduces a low-pressure region near the oil outlet, which may connect with the suction port and cause undesirable backflow. This backflow disrupts the pressure balance and reduces the volumetric efficiency of the pump. In addition, minor fluctuations in the pressure profile may occur due to this reverse flow. The Curved unloading groove, with its increased separation between inlet and outlet channels, effectively prevents such adverse flow communication. Consequently, pressure fluctuation is alleviated, and the overall pressure field becomes more uniform, demonstrating the improved hydraulic stability and effectiveness of the optimized groove design.

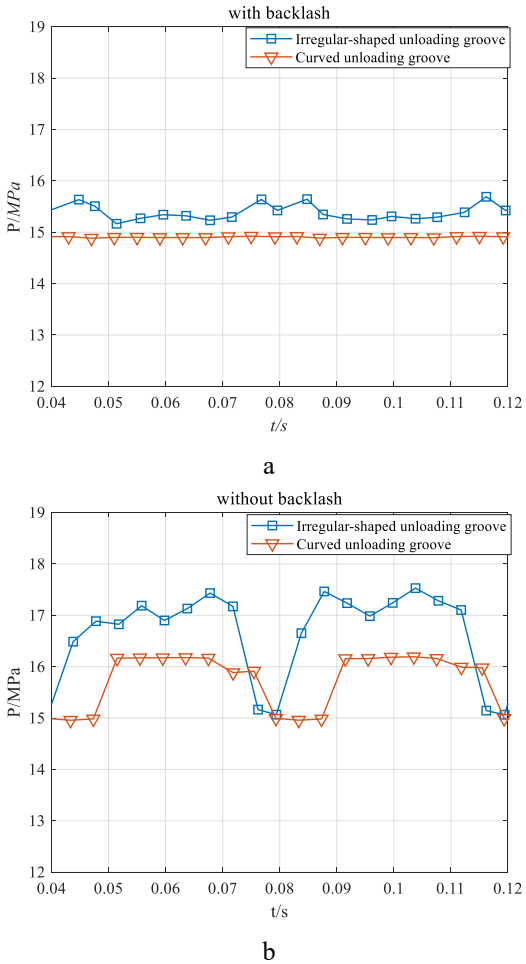


Fig. 14 The pressure of the oil trap zone of the fluid of different gear pumps: a – pressure value of oil trapped area of two kinds of unloading groove with backlash. b – pressure value of oil trapped area of two kinds of unloading groove without backlash

At the same time, output the pressure curve obtained from the monitoring points in the trapped oil area, and organize the maximum pressure value at each formation of the trapped oil area. In order to avoid the error in the initial

stage of simulation, the data of two cycles of rotation of the simulated gear pump from 0.04 s to 0.12 s is selected here.

It can be seen from Fig. 14 that in the absence of tooth backlash, the pressure in the trapped oil region associated with the Irregular-shaped unloading groove reaches a maximum of approximately 18 MPa, indicating severe pressure buildup due to incomplete pressure relief in isolated oil pockets. This phenomenon arises when one of the sealed regions is connected to the outlet while the other remains enclosed, preventing timely pressure release. In contrast, the Curved unloading groove reduces the peak pressure to about 15.5 MPa, reflecting a significant improvement in pressure relief effectiveness through symmetrical groove design and optimized spatial layout.

In the presence of tooth backlash, the Irregular-shaped unloading groove produces relatively moderate pressure levels in the trapped oil zone; however, localized fluctuations are observed, likely attributed to backflow between the suction and discharge regions. The Curved unloading groove effectively suppresses such fluctuations by preventing simultaneous communication between inlet and outlet ports. As a result, the pressure curve within the trapped oil zone exhibits improved stability, demonstrating enhanced dynamic behavior of the pump under backlash conditions.

### 4.2. Comparison of simulated and experimental flow data

To verify the performance of the optimized unloading groove structure under actual operating conditions, experimental data are compared with CFD simulation results to evaluate the fluid characteristic parameters of the optimized structure in the external gear pump. By measuring the outlet flow rates of gear pumps equipped with two different unloading groove structures, the real operating state of the internal flow can be reflected, and the effectiveness of the structural optimization can be further validated. Meanwhile, the experimental results are also used to verify the accuracy and reliability of the CFD simulation model.

The experimental test rig mainly consists of a motor, coupling, transmission shaft, plunger pump, external gear pump, suspension system, oil tank, relief valve, suction and discharge pipelines, flow sensors, and a data acquisition system. The working fluid used in the experiments is ISO VG 46 anti-wear hydraulic oil. During the experiments, oil temperature, fluid viscosity, and load pressure are strictly controlled to ensure consistency between the experimental conditions and actual operating conditions, thereby improving the engineering representativeness and reliability of the measured data.

The instantaneous flow signal at the outlet is collected in real time using flow and pressure sensors, providing complete time-domain flow data. These data serve as the basis for subsequent calculations and comparisons of average flow rate, volumetric efficiency, and flow non-uniformity coefficient.

In the CFD post-processing stage, instantaneous flow data are extracted from the outlet monitoring surface and then organized and statistically compared with the experimentally measured flow data obtained from the flow sensors, enabling a comprehensive validation of the consistency between the numerical model and the actual flow behavior.

As shown in Fig. 15, further analysis reveals that, compared with the Irregular-shaped unloading groove, the Curved unloading groove significantly reduces the fluctuation amplitude of the outlet flow rate over the entire operating cycle, resulting in a more continuous and stable flow output. This improvement is mainly attributed to the smooth arc transition of the Curved unloading groove, which enables a more gradual pressure relief process in the trapped oil region and effectively suppresses flow pulsations induced by abrupt pressure variations.

Under the condition with backlash, this stabilizing effect becomes even more pronounced. The presence of backlash intensifies internal leakage and flow disturbances, which tends to amplify flow fluctuations in the conventional structure. However, the Curved unloading groove partially

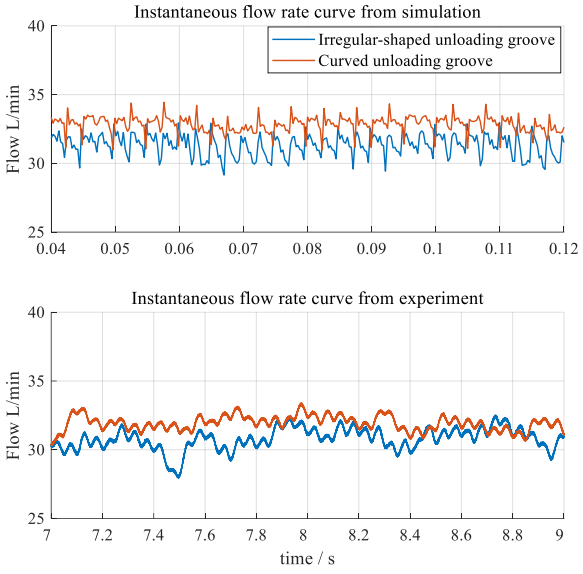


a

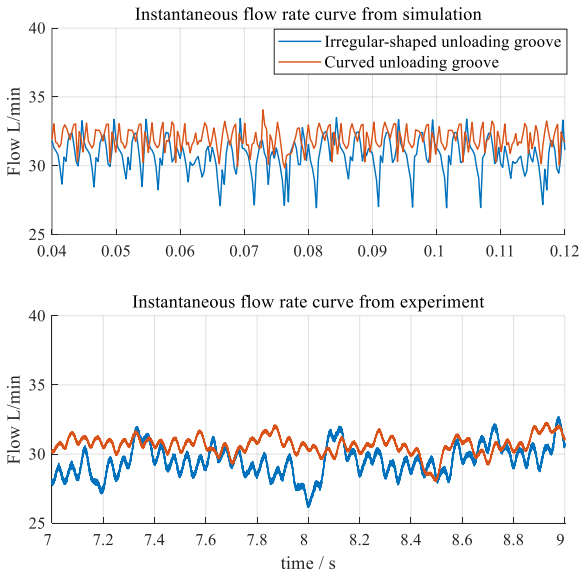


b

Fig. 15 Instantaneous flow rate curves of the irregular-shaped and curved unloading grooves in experiment and simulation: a – without backlash. b – with backlash

compensates for the instability introduced by backlash by optimizing the pressure release pathway of the trapped volume, thereby significantly improving the uniformity and

stability of the outlet flow. Overall, the Curved unloading groove demonstrates a more prominent improvement in flow stability under complex backlash conditions.

The flow non-uniformity coefficient is used to analyze and evaluate the flow quality of the external gear pump [25]. When the flow non-uniformity coefficient of flow pulsation is larger, the flow pulsation of the external gear pump becomes more severe, resulting in stronger noise under the same load conditions.

The flow non-uniformity coefficient is the ratio of the difference between the maximum and minimum flow rates to the average value. It can intuitively reflect the smoothness of the flow pulsation at the inlet and outlet of a gear pump [26]. The instantaneous flow values of the inlet and outlet are obtained through simulation. Then, eliminating singular values caused by simulation errors, calculating the average flow rate, find the corresponding maximum value $Q_{max}$ and the minimum value $Q_{min}$ to calculate the flow non-uniformity coefficient. The flow nonuniformity coefficient is defined as

$$\delta_Q = \frac{Q_{max} - Q_{min}}{\bar{Q}} \times 100\%, \tag{22}$$

where $Q_{max}$ is the maximum instantaneous flow in a single rotation cycle; $Q_{min}$ is the minimum value of instantaneous flow; $\bar{Q}$ is the periodic average flow. If continuous monitoring is adopted, its expression is

$$\bar{Q} = \frac{1}{T}\int_0^T Q(t)dt, \tag{23}$$

where $T$ is the rotation cycle of the gear.

If discrete sampling is adopted, the expression is

$$\bar{Q} = \frac{1}{N}\sum_{i=1}^{N} Q_i, \tag{24}$$

where $N$ is the quantity set of samples.

Table 5

Flow data indices of the oil outlet under the case of irregular-shaped unloading groove

| | | Without backlash | | With backlash | |
|---|---|---|---|---|---|
| | | Volumetric efficiency | Flow non-uniformity coefficient | Volumetric efficiency | Flow non-uniformity coefficient |
| Irregular-shaped unloading groove | experiment | 0.877 | 0.149 | 0.840 | 0.223 |
| | simulation | 0.892 | 0.122 | 0.875 | 0.213 |
| Curved unloading groove | experiment | 0.909 | 0.097 | 0.873 | 0.139 |
| | simulation | 0.935 | 0.105 | 0.911 | 0.132 |

The flow data index of the oil outlet corresponding to the Irregular-shaped unloading groove and Curved unloading groove are given in Tables.

By comparing the data presented in Table 5, it can be concluded that operating conditions without backlash generally exhibit better performance in terms of volumetric efficiency and flow non-uniformity coefficient compared with those with backlash. This indicates that the presence of backlash increases internal leakage and flow disturbances, thereby reducing volumetric utilization and aggravating outlet flow fluctuations in the gear pump.

Further analysis shows that under conditions with backlash, the Curved unloading groove demonstrates a more significant improvement in flow stability compared to the Irregular-shaped unloading groove. This is mainly attributed to its smoothly varying geometric transition, which optimizes the pressure release path of the trapped oil volume, effectively mitigating the additional leakage and pressure pulsation induced by backlash, and thus leading to a more stable flow output.

In addition, the comparison between simulation and experimental results under identical operating conditions shows that the relative error is generally within 0.05, indicating a high level of agreement. This not only validates the reliability of the CFD model in predicting the flow characteristics of the gear pump, but also further confirms the effectiveness and practical performance improvement of the Curved unloading groove in engineering applications.

It should be noted that a certain degree of measurement uncertainty is unavoidable in the experimental process. The main sources of uncertainty include the accuracy and calibration error of the flow sensors, the resolution of the data acquisition system, fluctuations in oil temperature and viscosity, as well as manufacturing and assembly tolerances of the gear pump components. In particular, small variations in tooth backlash, side-plate clearance, and unloading groove dimensions may affect the actual leakage characteristics and pressure-relief behavior, thereby introducing deviations between the numerical and experimental results.

To reduce the influence of these factors, all experiments were conducted under carefully controlled operating conditions, with the oil temperature, rotational speed, and outlet pressure maintained as constant as possible throughout the testing process. In addition, repeated measurements were performed to ensure the repeatability and consistency of the acquired data. Considering the combined effects of experimental uncertainty and numerical modeling assumptions, the observed deviation between simulation and experiment remains within an acceptable range. Therefore, the CFD model can be regarded as sufficiently accurate for capturing the pressure-relief mechanism and flow characteristics of the optimized unloading groove, providing a reliable basis for the structural optimization and performance evaluation of the external gear pump.

## 5. Conclusions

This work is based on a specific model of an external gear pump and centers on the optimization of the fluid dynamic design of the unloading groove, with a particular focus on operating conditions both with and without tooth backlash. SolidWorks is employed to construct the physical models incorporating different configurations of the unloading groove, while PumpLinx is utilized to simulate the

internal flow fields. Through numerical simulation, critical performance indicators – including pressure distribution, trapped oil pressure, flow pulsation, and volumetric efficiency – are extracted and comparatively analyzed.

The performance of the original Irregular-shaped unloading groove and the Curved unloading groove is systematically evaluated under both backlash and non-backlash scenarios. The conclusions of this study are as follows:

1. Under conditions without tooth backlash, the Curved unloading groove significantly enhances flow stability while maintaining high volumetric efficiency. It effectively mitigates the pressure buildup in the trapped oil zone, thereby improving overall hydraulic performance.

2. In the presence of tooth backlash, the Curved unloading groove substantially reduces pressure pulsation in the trapped oil region and alleviates flow pulsation, contributing to smoother and more efficient pump operation.

3. For the dynamically optimized Curved unloading groove, the pressure pulsation in the trapped oil region remains relatively consistent between the backlash and non-backlash conditions. However, the average flow rate is lower when backlash is present, although the corresponding flow pulsation is notably reduced.

These findings demonstrate that the Curved unloading groove contributes positively to the dynamic performance of external gear pumps across different structural conditions. Given that achieving minimal tooth backlash requires high-precision manufacturing – which entails additional cost – it is recommended that the selection of backlash tolerances for pumps equipped with the Curved unloading groove be adapted according to actual operational requirements and economic considerations.

Based on the simulation and experimental results, we propose the following systematic design suggestions

1. Dynamic compensation and adaptive design

The initial setting of backlash should take into account both static assembly accuracy and dynamic operation characteristics. It is recommended to use the micron precision clearance benchmark, with the leakage suppression as the dominant constraint, and fully consider the thermal expansion and elastic deformation effect of the gear pair under high speed and high pressure. Through the selection of low expansion materials and the design of elastic support structure, the thermal mechanical coupling adaptive mechanism is constructed to dynamically adjust the gap value with the change of temperature and pressure, so as to avoid interference stagnation or out of control gap.

2. Multi parameter collaborative optimization

The tooth backlash needs to be designed in coordination with key parameters such as the layout of the unloading groove and the tooth tip clearance. The geometric characteristics of the unloading groove should dominate the trapped oil pressure relief path to avoid the backlash becoming the main leakage channel. The two need to form a functional complement through the area ratio of the channel. The ratio of tip clearance to backlash needs to be coordinated and optimized to establish a balance between preventing the friction of sweeping bore and restraining the leakage of end face. It is suggested to adopt the multi-objective optimization algorithm to synchronously iterate the clearance parameters and the macro geometry of the gear, so as to comprehensively improve the efficiency, pressure stability and noise performance.

**Acknowledgements**

The work is supported by the Priority Academic Program Development of Jiangsu Higher Education Institutions.

**References**

1. **Frosina, E.; Senatore, A.; Rigosi, M.** 2017. Study of a High-Pressure External Gear Pump with a Computational Fluid Dynamic Modeling Approach, Energies 10(8): 1113. https://doi.org/10.3390/en10081113.
2. **Guerra, D.; Polastri, M.; Battarra, M.; Suman, A.; Mucchi, E.; Pinelli, M.** 2021. Design Multistage External Gear Pumps for Dry Sump Systems: Methodology and Application, Mathematical Problems in Engineering 2021(1): 8888128. https://doi.org/10.1155/2021/8888128.
3. **Nath, A. G.; Krishnan, E. S.; Cheriyan, S.; Vishnu, P. S.; Krishnan, A.; Sreedharan, P.; Udupa, G.** 2018. Design and Manufacture of Miniature Hydraulic Gear Pump for Bio-Medical Application, Materials Today: Proceedings 5(11): 25570-25580. https://doi.org/10.1016/j.matpr.2018.10.364.
4. **Thiagarajan, D.; Vacca, A.; Watkins, S.** 2019. On the lubrication performance of external gear pumps for aerospace fuel delivery applications, Mechanical Systems and Signal Processing 129: 659-676. https://doi.org/10.1016/j.ymssp.2019.04.030.
5. **Corvaglia, A.; Ferrari, A.; Rundo, M.; Vento, O.** 2021. Three-dimensional model of an external gear pump with an experimental evaluation of the flow ripple, Proceedings of the Institution of Mechanical Engineers, Part C: Journal of Mechanical Engineering Science 235(6): 1097-1105. https://doi.org/10.1177/0954406220937043.
6. **Kim, J. H.; Kim, S. G.** 2013. The Flow Rate Characteristics of External Gear Pump for EHPS, in 2013 4th International Conference on Intelligent Systems, Modelling and Simulation: 346-349. https://doi.org/10.1109/ISMS.2013.113.
7. **Huang, K.; Han, G.; Xiong, Y.; Cheng, Z.; Sang, M.** 2023. Design and fluid analysis of the microsegment gear tooth profile for pump operating at high speed and high pressure, Proceedings of the Institution of Mechanical Engineers, Part E: Journal of Process Mechanical Engineering 239(3): 1415-1430. https://doi.org/10.1177/09544089231190181.
8. **Antoniak, P.; Stryczek, J.** 2018. Visualization study of the flow processes and phenomena in the external gear pump, Archives of Civil and Mechanical Engineering 18(4): 1103-1115. https://doi.org/10.1016/j.acme.2018.03.001.
9. **Liang, Y.; Chen, Z.; Liao, J.** 2022. Numerical simulation and experimental evaluation of flow ripple characteristics of Truninger pump, Scientific Reports 12(1): 11297. https://doi.org/10.1038/s41598-022-15452-8.
10. **Zhou, Y.; Li, W.; Yang, D.** 2018. Noise Simulation Analysis of a Variable Displacement External Gear Pump and Unloading Groove Optimization, Open Access Library Journal 5(11): 1-9.
11. **Zhang, H.; Zhan, D. Y.; Tian, R. Q.; Zhang, T. A.**

2023. Study on Multi-flow Field Characteristics of Unloading Groove Spacing of Bidirectional Gear Pump, Journal of Applied Fluid Mechanics 16(5): 1089-1098. https://doi.org/10.47176/jafm.16.01.1591.
12. **Zhan, P.; Qiang, Y.; Jiang, Z.; Yang, R.; Wei, L.** 2024. Study on Mechanism and Suppression Method of Flow-Induced Noise in High-Speed Gear Pump, Archives of Acoustics 49(1): 49-60. https://doi.org/10.24425/aoa.2023.146824.
13. **Liu, H.; Pan, M.; Fu, J.; Li, H.; Cao, R.** 2022. A New Type Unloading Groove Design and Simulation for Engine Fuel Gear Pump, in 2022 13th International Conference on Mechanical and Aerospace Engineering (ICMAE): 86-90. https://doi.org/10.1109/ICMAE56000.2022.9852515.
14. **Sedri, F.; Riasi, A.** 2019. Investigation of leakage within an external gear pump with new decompression slots: numerical and experimental study, Journal of the Brazilian Society of Mechanical Sciences and Engineering 41: 224. https://doi.org/10.1007/s40430-019-1717-8.
15. **Gamez-Montero, P. J.; Garcia-Vilchez, M.; Raush, G.; Freire, J.; Codina, E.** 2012. Teeth Clearance and Relief Grooves Effects in a Trochoidal-Gear Pump Using New Modules of GeroLAB. ASME Journal of Mechanical Design 134(5): 054502. https://doi.org/10.1115/1.4006440.
16. **Szwemin, P.; Fiebig, W.** 2021. The Influence of Radial and Axial Gaps on Volumetric Efficiency of External Gear Pumps, Energies 14(15): 4468. https://doi.org/10.3390/en14154468.
17. **Peng, Z.; Liejiang, W.; Rongmin, L.; Mingyuan, L.; Yan, Q.** 2023. Flow Field Modeling and Simulation of High-Speed Gear Pump Considering Optimal Radial and End Clearance, IEEE Access 11: 64725-64737. https://doi.org/10.1109/ACCESS.2023.3290079.
18. **Gamez-Montero, P. J.; Castilla, R.; del Campo, D.; Ertürk, N.; Raush, G.; Codina, E.** 2012. Influence of the interteeth clearances on the flow ripple in a gerotor pump for engine lubrication, Proceedings of the Institution of Mechanical Engineers, Part D: Journal of Automobile Engineering 226(7): 930-942. https://doi.org/10.1177/0954407011431545.
19. **Zou, X.; Yang, C.; Liu, B.** 2020. The Contact and Transient Dynamic Analysis of Gear Meshing with ANSYS, Open Access Library Journal 7(9): 1-10.
20. **Li, Y. L.; Liu, K.; Sun, F. C.** 2012. Dynamic Model of Gears with Trapped Oil and Coupled Analysis in External Spur-Gear Pump, Applied Mechanics and Materials 130-134: 610-615. https://doi.org/10.4028/www.scientific.net/AMM.130-134.610.
21. **Campo Sud, D. D.** 2012. Analysis of the suction chamber of external gear pumps and their influence on cavitation and volumetric efficiency. Tesi doctoral, UPC, Departament de Mecànica de Fluids. https://doi.org/10.5821/dissertation-2117-94595
22. **Li, G.; Zhang, L.; Han, W.** 2018. Profile design and displacement analysis of the low pulsating gear pump, Advances in Mechanical Engineering 10(3): 1687814018767003. https://doi.org/10.1177/1687814018767003
23. **El-Hadj, A. A.; Abd Rahim, S. Z. B.** 2020. Optimization of an External Gear Pump using Response Surface Method, Journal of Mechanics 36(4), 567-575. https://doi.org/10.1017/jmech.2020.7.
24. **Qi, F., Dhar, S.; Nichani, V. H.; Srinivasan, C.; Wang, D. M.; Yang, L.; Bing, Z.; Yang, J. J.** 2016. A CFD study of an Electronic Hydraulic Power Steering Helical External Gear Pump: Model Development, Validation and Application, SAE International Journal of Passenger Cars-Mechanical Systems 9(1): 346-352. https://doi.org/10.4271/2016-01-1376.
25. **Tankasala, S.; Vacca, A.** 2019. Theoretical Analysis and Design of a Variable Delivery External Gear Pump for Low and Medium Pressure Applications, ASME Journal of Mechanical Design 141(1): 013401. https://doi.org/10.1115/1.4041351.
26. **Zhao, X.; Vacca, A.** 2017. Numerical analysis of theoretical flow in external gear machines, Mechanism and Machine Theory 108: 41-56. https://doi.org/10.1016/j.mechmachtheory.2016.10.010.

J.C. Tang, M.Y. Lan, L. Zhao, S.B Zhang, J.H. Yang, Z. Shan

OPTIMIZATION DESIGN OF FLUID DYNAMIC PERFORMANCES OF EXTERNAL GEAR PUMP

S u m m a r y

External gear pump is a commonly used pump in hydraulic transmission system, and its dynamical performance directly affects the working stability and efficiency of the system. The tooth backlash is one of the important factors influencing the flow pulsation of the external gear pump, and the design of the unloading groove is an important measure to alleviate the oil trapping phenomenon, which can effectively alleviate the pressure of the oil trapping area, and will also have a certain effect on the flow pulsation and pressure pulsation, and the effect of different kinds of unloading grooves is also different. In this work, the software PumpLinx is applied to simulate the fluid dynamics of the gear pump equipped with an irregular-shaped unloading groove in the presence or absence of tooth backlash. The optimal design of the unloading groove is carried out to improve the performance of the gear pump to a certain extent. The results of this study have important reference value for the dynamic design and optimization of external gear pumps.

**Keywords:** fluid dynamics, external gear pump, dynamic design, tooth backlash, flow pulsation.

Received July 24, 2025
Accepted June 19, 2026

This article is an Open Access article distributed under the terms and conditions of the Creative Commons Attribution 4.0 (CC BY 4.0) License (http://creativecommons.org/licenses/by/4.0/).